ELSEVIER

Biochimica et Biophysica Acta 1328 (1997) 243–260

BIOCHIMICA ET BIOPHYSICA ACTA
BBA

Conducting and voltage-dependent behaviors of the native and purified SR Ca^{2+}-release channels from the canine diaphragm [1]

Maryse Picher, Anne Decrouy [2], Sonia Proteau, Eric Rousseau [*]

Department of Physiology and Biophysics, Faculty of Medicine, University of Sherbrooke, 3001, 12 avenue North, Sherbrooke, QC, Canada J1H 5N4

Received 14 April 1997; accepted 28 April 1997

Abstract

The ryanodine-sensitive Ca^{2+}-release channel of the canine diaphragm sarcoplasmic reticulum (SR) was characterized using biochemical assays and the planar lipid bilayer technique. Diaphragm SR membranes have a [^{3}H]ryanodine-binding capacity (B_{max}) of 1.2 pmol/mg protein and a binding affinity (K_D) of 6.3 nM. The conductance of the native channel was 330 pS in 50 mM/250 mM *trans/cis* $CsCH_3SO_3$ and was reduced to 71 pS by 10 mM Ca^{2+} *trans*. The Ca^{2+}-release channel was purified as a 400 kDa protein on SDS-PAGE and displayed a conductance of 715 pS in 200 mM KCl. The native and purified Ca^{2+} channels were activated by micromolar Ca^{2+} and ATP and inhibited by Mg^{2+}, ryanodine and ruthenium red. Although diaphragm muscle contraction was shown to depend on extracellular Ca^{2+} like cardiac muscles, we provide evidence that the diaphragm SR Ca^{2+}-release channel may be classified as a skeletal ryanodine receptor isoform. First, the IC_{50} for [^{3}H]ryanodine binding was in the same range as estimated for skeletal SR, with 20 nM. Second, the channel was maximally activated by 10–30 μM cytoplasmic Ca^{2+} and inhibited at higher concentrations. Third, ryanodine binding to the diaphragm SR was less sensitive to Ca^{2+} than cardiac SR, with EC_{50} values of 50 and 1 μM, respectively. Finally, Ca^{2+}-release activity and [^{3}H]ryanodine binding capacity of the diaphragm and skeletal SR were similarly more sensitive to Mg^{2+} than cardiac SR. Together, these results suggest a predominantly skeletal-type of excitation-contraction coupling in the diaphragm. © 1997 Elsevier Science B.V.

Keywords: Diaphragm; Calcium channel; Ryanodine receptors; Skeletal muscles; Excitation–contraction coupling

1. Introduction

In striated muscle cells, the sarcoplasmic reticulum (SR) is responsible for the release and uptake of Ca^{2+} during excitation-contraction coupling (ECC) [1,2]. The release of Ca^{2+} from the SR is mediated by Ca^{2+}-release channels, also known as ryanodine receptors (RyRs), because they bind to the plant alkaloid with high affinity and specificity [3,4]. Three structurally related RyRs have been identified in mammalian tissues: a skeletal muscle (RyR_1) isoform

* Corresponding author. Tel: +1-819-5645306; fax: +1-819-5645399; e-mail: e.rousse@courrier.usherb.ca.

[1] The first two authors contributed equally to the present work. A.D. generated the idea and the basic electrophysiological data. M.P. recorded complementary data and wrote the manuscript, while S.P. performed the biochemical experiments and E.R. supervised the project.

[2] Present address: Department of Physiology, Faculty of Medicine, University of Ottawa, 451 Smyth road, Ottawa, Ont., Canada K1H 8M5.

PII S0005-2736(97)00104-1

[5], a cardiac muscle (RyR_2) isoform [6,7] and a third isoform (RyR_3) first detected in the brain [8]. All three isoforms have structural and functional features in common. They migrate through sucrose gradients with an apparent sedimentation coefficient of ~30 S [9] and they display a major polypeptide band of ~400 kDa on SDS-polyacrylamide gels [10–12]. The functional channel is formed by four of these ~400 kDa proteins [13], which have been shown to correspond to the 'foot proteins' that span the gap between the SR membrane and the T-tubule [6,14]. The very large subunits presumably allow a complex pattern of regulation by various endogenous and exogenous effector molecules. The cardiac and skeletal Ca^{2+}-release channels are activated by micromolar Ca^{2+}, ATP, caffeine and nanomolar ryanodine and they are inhibited by Mg^{2+}, ruthenium red and micromolar ryanodine [15]. A number of differences however attest that the RyR isoforms are not equivalent. They are expressed by three different genes and they share only 67% amino acid sequence identity [8,16]. The cardiac and skeletal isoforms differ in their sensitivity to cytoplasmic Ca^{2+} [17–20] and to phosphorylation by calmodulin- and cyclic AMP-dependent protein kinases [21,22]. Finally, two different mechanisms of RyR activation have been postulated for skeletal and cardiac muscles: RyRs 'physically' coupled to voltage-dependent dihydropyridine-sensitive Ca^{2+} channels (DHPRs) of the sarcolemmal T-tubules [23] and RyRs activated by an influx of extracellular Ca^{2+} through DHPRs [24,25].

Although the diaphragm has been classified as a striated skeletal muscle, this tissue shares contractile properties with both the cardiac and non-respiratory skeletal muscles. Like the heart, the diaphragm contracts rhythmically for life. On the other hand, it responds to neural drive as well as work load very much like skeletal muscles [26]. Despite numerous studies dealing with the contractile properties of normal and dystrophic diaphragm fibers [27–30], little is known of the electrophysiological properties of their SR membrane system. Muscle contraction was shown to rely on extracellular Ca^{2+} [31,32] and to be altered by ryanodine [33,34]. Recent studies have reported the functional characteristics of the SR Ca^{2+} pump [35] and the SR conductance for monovalent ions [36]. In this study, we investigated the Ca^{2+}-releasing properties of the diaphragm SR using biochemical assays and single-channel recordings from SR vesicles or purified ryanodine receptors incorporated into planar lipid bilayers.

2. Materials and methods

2.1. Materials

AMP (adenosine 5′-monophosphate), ATP (adenosine 5′-triphosphate), $CaCl_2$, cesium methanesulfonate ($CsCH_3SO_3$), dithio-threitol, $MgSO_4$ and protease inhibitors were obtained from Sigma (St. Louis, Mo). Ruthenium red was bought from Terochem, AEBSF (4-(2-aminoethyl)-benzenesulfonyl fluoride) from Boehringer Mannheim and phospholipids from Avanti Polar-lipids (Alabaster, Al). [^{3}H]ryanodine was purchased from New England Nuclear (NEN-Dupont Canada) and cold ryanodine was kindly provided by Dr. L. Ruest, Department of Chemistry, University of Sherbrooke, Canada. Deionized water from a Millipore Ro-Milli-Q-UF system (18 ± 0.2 MΩ/cm^2) was used to prepare all buffer solutions. All other chemicals were commercial products of analytical grade.

2.2. Preparation of sarcoplasmic reticulum vesicles and purified ryanodine receptors

Microsomal fractions enriched in SR vesicles were prepared from canine diaphragm according to Rousseau et al. [37]. Briefly, canine diaphragms were homogenized and centrifuged at 7,500 rpm ($6{,}000 \times g$) for 20 min at 4°C in Tris–maleate buffer (pH 6.8) in the presence of protease inhibitors. The supernatant was filtered and centrifuged at 33,000 rpm ($90{,}000 \times g$) at 4°C for 1 h 20 min. The pellet was resuspended in K-PIPES buffer (pH 7.0) and the membrane vesicles were separated by ultracentrifugation at $120{,}000 \times g$ on a 25–45% sucrose gradient. Sucrose fractions were analyzed for their protein content and [^{3}H]ryanodine binding activity. Protein concentration was determined by the Lowry method [38] using bovine serum albumin as a standard. [^{3}H]ryanodine binding assays were performed using a procedure originally described by Hawkes et al. [39] and routinely used in our laboratory [40]. Briefly,

microsomal fractions (100 μg) collected from the sucrose gradient were incubated 90 min at 37°C in the presence of 1 M NaCl, 5 mM AMP, 50 μM free Ca^{2+}, 20 mM MOPS and 5 nM [^{3}H]ryanodine. The mixture was then centrifuged twice and pellet radioactivity was determined by liquid scintillation. Specific [^{3}H]ryanodine binding was calculated by subtracting nonspecific binding (5 nM [^{3}H]ryanodine + 5 μM ryanodine) from total binding (5 nM [^{3}H]ryanodine). The saturation curves were fitted with the following equation $y = ax/(b + x)$ describing the Michaelis–Menten formalism where a is the maximum value (B_{max}) and b the dissociation constant (K_D). The displacement curves were obtained in the presence of increasing concentrations of unlabelled ryanodine. The mean values obtained from the displacement experiments were fitted with the following equation: $y = (a - d)/(1 + (x/c)^b) + d$, where a is the asymptotic maximum, b is the slope, c is the value of inflection (half displacement) and d is the asymptotic minimum.

The most enriched fraction in ryanodine receptors, recovered in 40% sucrose, was used to purify the SR Ca^{2+}-release channel. The microsomal fraction was incubated with [^{3}H]ryanodine, solubilized in 1% CHAPS and 3% azolectine and finally subjected to centrifugation in a linear 5–25% (w/v) sucrose density gradient [12]. The sucrose fractions were again analyzed for their [^{3}H]ryanodine binding activity and protein content.

2.3. Immunoblot assays

Microsomes were electrophoresed on 6% SDS-PAGE gels and transferred to nitrocellulose membranes at 30 V overnight at 4°C. The nitrocellulose membranes were washed 15 min in 200 mM Tris, 1.4 M NaCl + 0.1% Tween 20, pH 7.6 (TBS-T), blocked with 5% non-fat dry milk in TBS-T and incubated with polyclonal antibodies raised against the skeletal ryanodine receptor isoform RyR_1 (kindly provided by Dr. Meissner, University of North Carolina). The membranes were incubated with donkey anti-rabbit IgG_1 secondary antibodies coupled to horseradish peroxidase (HRP) (Amersham) 1 h at 23°C and then detected with the HRP-precipitating reagent (Harlan Bioproducts).

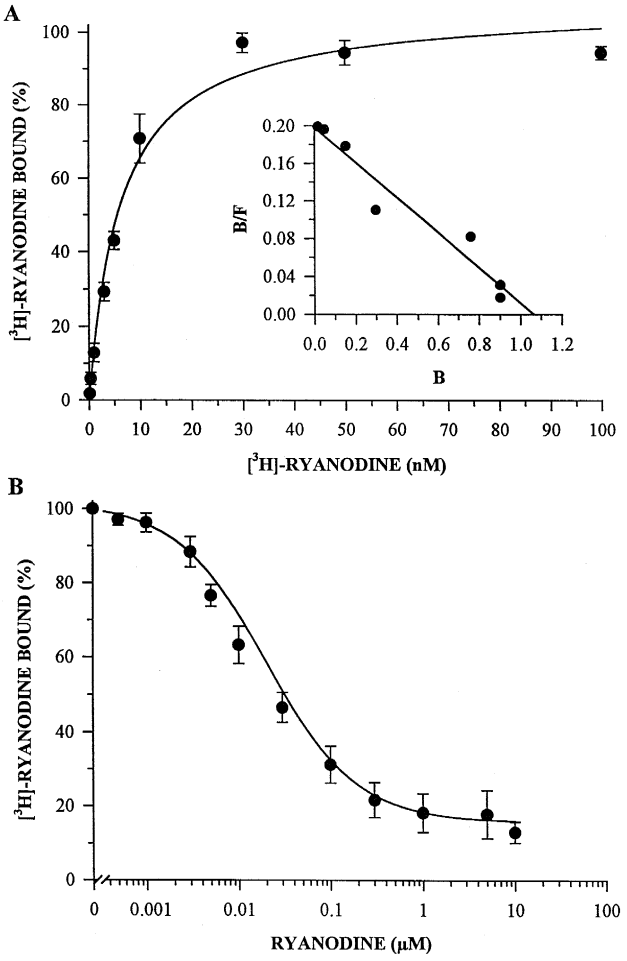

Fig. 1. Normalized equilibrium binding curve for the Ca^{2+}-release channel marker [^{3}H]ryanodine followed by Scatchard analysis and displacement experiments. (A) Saturation curve representing the mean of five independent determinations using increasing concentrations of radioactive ligand. Values were expressed in % of the maximum binding capacity (B_{max}). Inset: Typical Scatchard analysis of the bound (B) over bound/free (B/F) [^{3}H]ryanodine. K_d and B_{max} values were 6.3 nM and 1.06 pmol/mg of protein, respectively. (B) Displacement of [^{3}H]ryanodine bound to its receptor by unlabelled ryanodine. Each assay contained 5 nM [^{3}H]ryanodine, 100 μg of protein and increasing concentrations of cold ryanodine from 1 nM to 10 μM. Percentage of [^{3}H]ryanodine bound was plotted as a function of unlabelled ryanodine concentration. As the concentration of ryanodine increases, the quantity of tritiated ryanodine bound to the Ca^{2+}-release channel decreases. The data shown are means (±SEM) from five similar experiments performed in triplicate on various preparations. Curve fitting attests that the data can be described by an equation assuming a single high affinity binding site.

2.4. Bilayer formation and vesicle fusion

The planar lipid bilayers (PLB) were formed at room temperature from a lipid mixture containing phosphatidylethanolamine, phospha-tidylserine and phosphatidylcholine in a ratio of 3:2:1 [37]. The final lipid concentration was 25 mg/ml dissolved in decane. A 250 μm diameter hole, drilled in a Delrin cup, was pretreated with the same lipid mixture dissolved in chloroform. Using a Teflon stick, a drop of the decane lipid mixture was gently spread across the aperture in order to obtain an artificial membrane. Membrane thinning was assayed by applying a triangular wave test pulse. Typical capacitance values were 150–300 pF. The chambers on either side of the membrane were designated as *cis* (cytoplasmic) and *trans* (luminal). Aliquots of SR vesicles or purified ryanodine receptor complexes (30–60 μg of protein) were added to the *cis* chamber in close proximity to the bilayer. In the case of SR vesicles, the chambers contained 50 mM/250 mM *trans / cis* cesium methanesulfonate ($CsCH_3SO_3$), plus symmetrical 10 μM free Ca^{2+} (109 μM $CaCl_2$ + 100 μM Tris–EGTA) and 20 mM Tris–HEPES pH 7.4, unless specified otherwise. The use of Tris and HEPES as large impermeant cations and anions eliminated currents through K^+ and Cl^- channels that are present in native SR vesicles and become incorporated into the PLB along with the Ca^{2+}-release channel [41]. The fusions were either spontaneous, or facilitated by applying positive potentials across the bilayer [42]. The purified ryanodine receptors were fused in symmetrical 200 mM KCl, plus 10 μM free Ca^{2+} and 20 mM Tris–HEPES pH 7.2 and 2 mM ATP *cis*, unless specified otherwise. Free Ca^{2+} concentrations were calculated using an apparent stability constant of 1.543×10^{-7} (pH 7.4) for Ca–EGTA buffers and computer programs published by Fabiato [43], and verified experimentally with a Ca^{2+} electrode (KWIKCAL-WPI, Sarasota, FL) as previously described [44,45].

2.5. Recording instrumentation and statistical analyses

Command voltages were applied to the PLB through Ag–AgCl electrode pellets connected to the chambers via 2 M KCl-fritted glass bridges (MERE2-WPI). The low impedence electrodes are very stable, they have minimized junction potentials and variability with time. The currents were recorded using a low noise amplifier (Dagan 3900), filtered (cut-off frequency 5 kHz) and recorded on a digital audio tape recorder through a pulse code modulation device (75 ES-SONY, Unitrade). The currents were simultaneously displayed on-line on a chart recorder (DASH II MT, Astro Med.) and an oscilloscope (Kikusui, 5020A). Current recordings were played back, filtered at 550 Hz with an 8-pole Bessel filter, sampled at 2 kHz for storage and analysed on an IBM Pentium computer using an Axotape program and the interface from Axon-Instrument. The open probability values (P_o) were determined from data stored in 60 to 120 s duration files unless specified otherwise and the half-threshold discriminator method was used. Applied voltages were defined with respect to the *trans* chamber, which was held at virtual ground. Average values were given as means $\pm$ standard error of the mean (SEM). Regression curves and curve-fittings were performed using the Windows version of the Sigma Plot program from Jandel Scientific.

Fig. 2. Biophysical properties of the native diaphragm SR Ca^{2+}-release channel. (A) Steady state currents of a single channel recorded at various holding potentials in 50/250 mM *trans/cis* $CsCH_3SO_3$, plus 10 μM free Ca^{2+} (109 μM $CaCl_2$ + 100 μM EGTA), 20 mM Tris–HEPES pH 7.4 and 2 mM Na_2ATP *cis*. Triangles on the right indicate the zero-current level. (B) Mean ($\pm$SEM) current/voltage relationships ($n = 4$) in 50/250 mM (▼) and 250/250 mM (◆) *trans/cis* $CsCH_3SO_3$: the mean channel conductances were 332 $\pm$ 24 pS and 298 $\pm$ 19 pS and the reversal potentials were -31.5 ± 3.2 mV and 0 mV, respectively. (C) Current/voltage curves in 50/250 mM *trans/cis* $CsCH_3SO_3$, 10 μM free Ca^{2+}, 20 mM Tris–HEPES (pH 7.4) and 2 mM Na_2ATP *cis*, showing modifications in the unitary conductance upon addition of 5 mM (○) or 10 mM (□) Ca^{2+} in the *trans* chamber. Unitary conductances in 10 μM, 5 and 10 mM Ca^{2+} *trans* were 421 pS, 364 pS and 382 pS in the positive voltage range, and 225 pS, 125 pS and 71 pS in the negative voltage range, respectively.

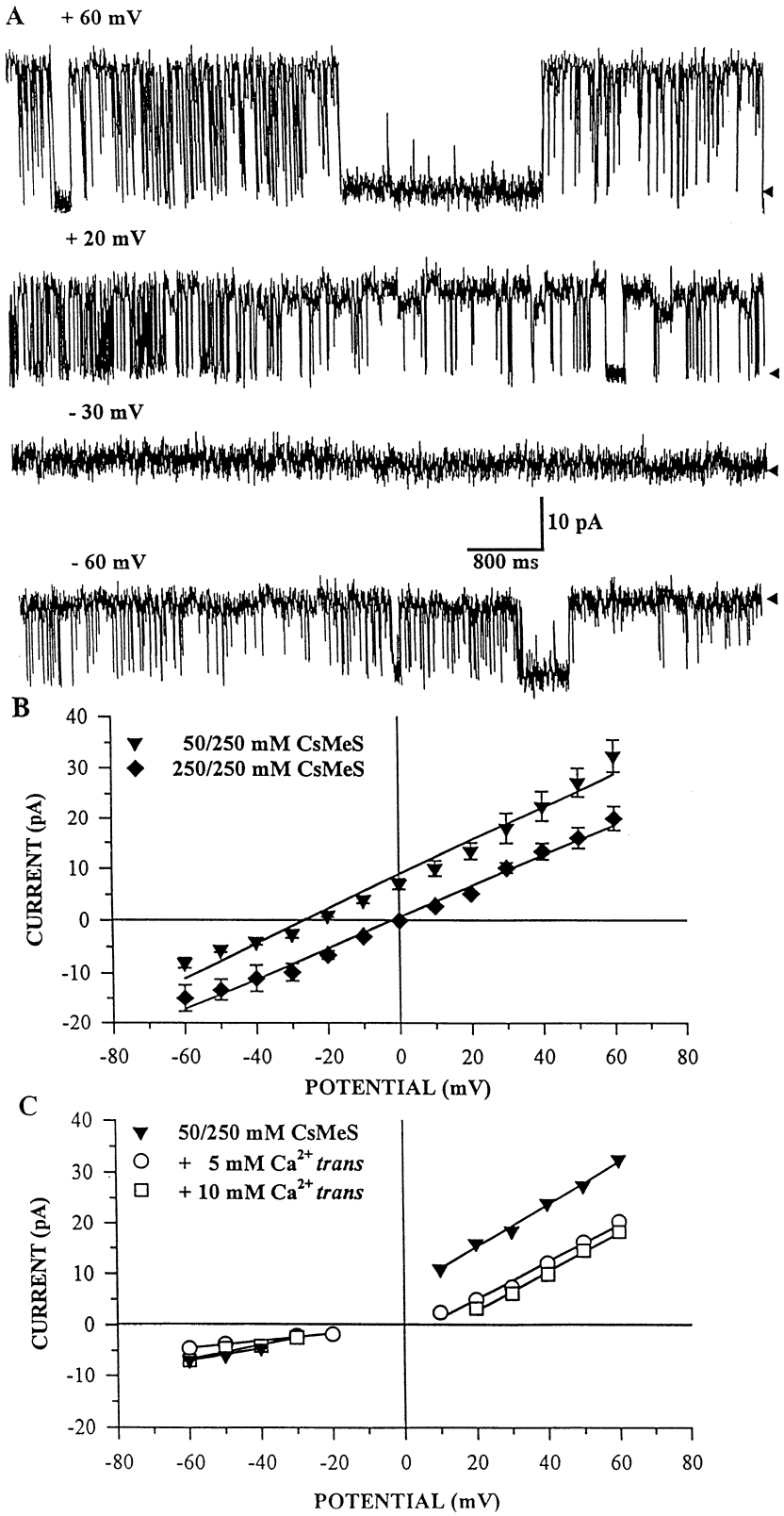
A
+ 60 mV
+ 20 mV
- 30 mV
10 pA
800 ms
- 60 mV
B
50/250 mM CsMeS
250/250 mM CsMeS
CURRENT (pA)
POTENTIAL (mV)
C
50/250 mM CsMeS
+ 5 mM Ca2+ trans
+ 10 mM Ca2+ trans
CURRENT (pA)
POTENTIAL (mV)

3. Results

3.1. Characterization of the diaphragm SR membrane vesicles

Diaphragm cell membranes were separated on a 25–45% step sucrose gradient and characterized using [^{3}H]ryanodine as a specific ligand for the SR Ca^{2+}-release channel [7,39,46]. The most enriched fraction in ryanodine receptors, which was recovered in 40% sucrose [36], was used in all biochemical and biophysical experiments. The affinity of the diaphragm SR Ca^{2+}-release channel for [^{3}H]ryanodine was evaluated under optimum conditions: high salt concentration (1 M NaCl), micromolar free Ca^{2+} (50 μM) and millimolar nucleotides (5 mM AMP) [17]. [^{3}H]ryanodine binding was studied with concentrations in the nanomolar range in order to address only

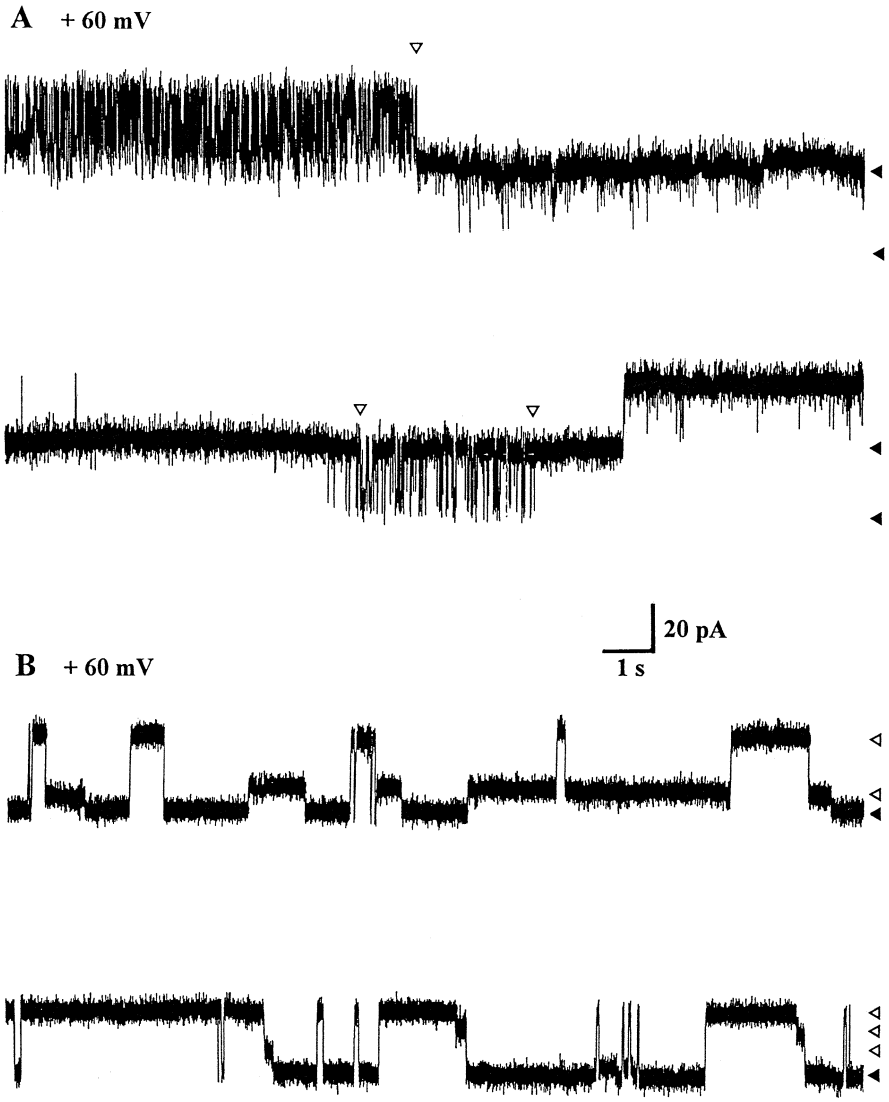

Fig. 3. Gating properties of the diaphragm SR Ca^{2+}-release channel. (A) Steady state currents of two channels recorded at a holding potential of +60 mV in 50/250 mM *trans/cis* $CsCH_3SO_3$, 20 mM Tris–HEPES, 10 μM free Ca^{2+} (109 μM $CaCl_2$ + 100 μM EGTA) pH 7.4. Open triangles above the traces indicate abrupt changes in gating, and filled triangles on the right indicate the zero-current level of the two channels. (B) Steady state current of a single channel recorded under the same conditions. Open triangles on the right indicate subconductance levels at 1/4, 1/2 and 3/4 of the conductance of the fully open state, and filled triangles indicate the zero-current level.

the high-affinity binding sites. Fig. 1A shows that the diaphragm SR binds [^{3}H]ryanodine in a saturable manner, with threshold and optimal concentrations of 1 and 50 nM, respectively. Scatchard analysis yields a straight line with a dissociation constant (K_D) of 6.3 nM and maximum binding value (B_{max}) of 1.2 pmol/mg of protein (Fig. 1A, inset). In cardiac and skeletal muscles, B_{max} values were reported in the range of 1 to 10 pmol/mg protein and 8 to 23 pmol/mg protein, respectively [13,21,47–50]. Fig. 1B indicates that increasing concentrations of unlabelled ryanodine (1 nM to 10 μM) displaced [^{3}H]ryanodine from its binding sites. Considering 14% non-specific binding, the concentration of unlabelled ryanodine needed to displace 50% of [^{3}H]ryanodine (IC_{50}) was estimated to be 20 nM. This value is similar to those reported for skeletal SR [10], but higher than the IC_{50} (5.2 nM) reported for cardiac SR [40].

3.2. Biophysical properties of the native Ca^{2+}-release channel

The experimental approach used to study the activity of the native diaphragm SR Ca^{2+}-release channel involved the incorporation of SR vesicles into planar lipid bilayers (PLB). Fig. 2A shows typical single-channel current fluctuations in 50/250 mM *trans/cis* $CsCH_3SO_3$, activated by symmetrical 10 μM free Ca^{2+} and 2 mM ATP *cis*. Under these conditions, Cs^+ is the permeant ion which flows from the *cis* to the *trans* chamber at voltages more positive than the reversal potential (−31.5 mV). For potentials more negative than −31.5 mV, currents are shown as downward deflections.

Fig. 2B presents current/voltage relationships recorded in 250/250 mM or 50/250 mM *trans/cis* $CsCH_3SO_3$. The mean slope conductance of the diaphragm channel was 317 ± 21 pS, which is less than the values reported for cardiac [51–53] and skeletal [54,55] channels (400–525 pS) in 250 mM Cs^+. In asymmetrical buffer systems, the reversal potential was shifted toward negative voltages, which argues in favor of a Cs^+ selectivity with respect to $CH_3SO_3^-$. The relative permeability of the diaphragm channel to monovalent and divalent cations was assessed in 50/250 mM *trans/cis* Cs^+ with increasing [Ca^{2+}] *trans* (Fig. 2C). Addition of millimolar Ca^{2+} to the *trans* chamber resulted in a deviation from the Ohmic current/voltage relationship that shifted the reversal potential toward more positive potentials. At positive potentials, the channel continued to conduct Cs^+ ions from the *cis* to the *trans* chamber in the presence of the two ionic species, due to the asymmetrical distribution of the Ca^{2+} ions. In the negative voltage range, the conductance was reduced to 71 pS by 10 mM Ca^{2+}, indicating that Ca^{2+} was competing with Cs^+ for the pore. Similar conductances were recorded with 50 mM Ca^{2+} *trans* (70–75 pS) for the cardiac SR channel [7,14,56], but higher values (100–120 pS) were obtained for the skeletal channel [12,37,54].

A permeability ratio of $P_{Ca^{2+}}/P_{Cs^+}$ of 14 was estimated from the field equation [57], where $[x]$ and $[y]$ correspond to the concentrations of Cs^+ and Ca^{2+}, while z, F, R and T have their usual meaning. This value is in the same range (10–30) as reported for the cardiac channel [20,51,58].

$$\frac{P_x}{P_y} = z^2 E \frac{F^2}{RT} \frac{[y]_i - [y]_o e^{(-zE(F/RT))}}{1 - e^{(-zE(F/RT))}} \times \left/ z^2 E \frac{F^2}{RT} \frac{[x]_i - [x]_o e^{(-zE(F/RT))}}{1 - e^{(-zE(F/RT))}} \right.$$

Most channels exhibited stationary gating properties composed of both long and short-lived events. About 15% of the channels underwent abrupt changes in gating behavior several times per minute (Fig. 3A). Similar mode switching behaviors were reported for cardiac and skeletal SR RyRs [18,20,58,59]. Subconductance levels at 1/4, 1/2 and 3/4 of the conductance of the fully open state were also reported in 10% of the recordings (Fig. 3B), as previously reported for skeletal [54,60,61] and cardiac [56] SR Ca^{2+}-release channels. Rapid flickering and subconductance levels at multiples of 25% of maximum have been suggested to reflect the loss of a regulatory protein called FK506-binding proteins (FKPBs) during the purification of SR membranes or RyRs [57].

3.3. Calcium sensitivity of the Ca^{2+}-release channel

The effect of cytoplasmic Ca^{2+} on the activity of the native channel was assayed under steady state conditions in 50/250 mM *trans/cis* $CsCH_3SO_3$. Fig. 4A shows the current fluctuations of a single

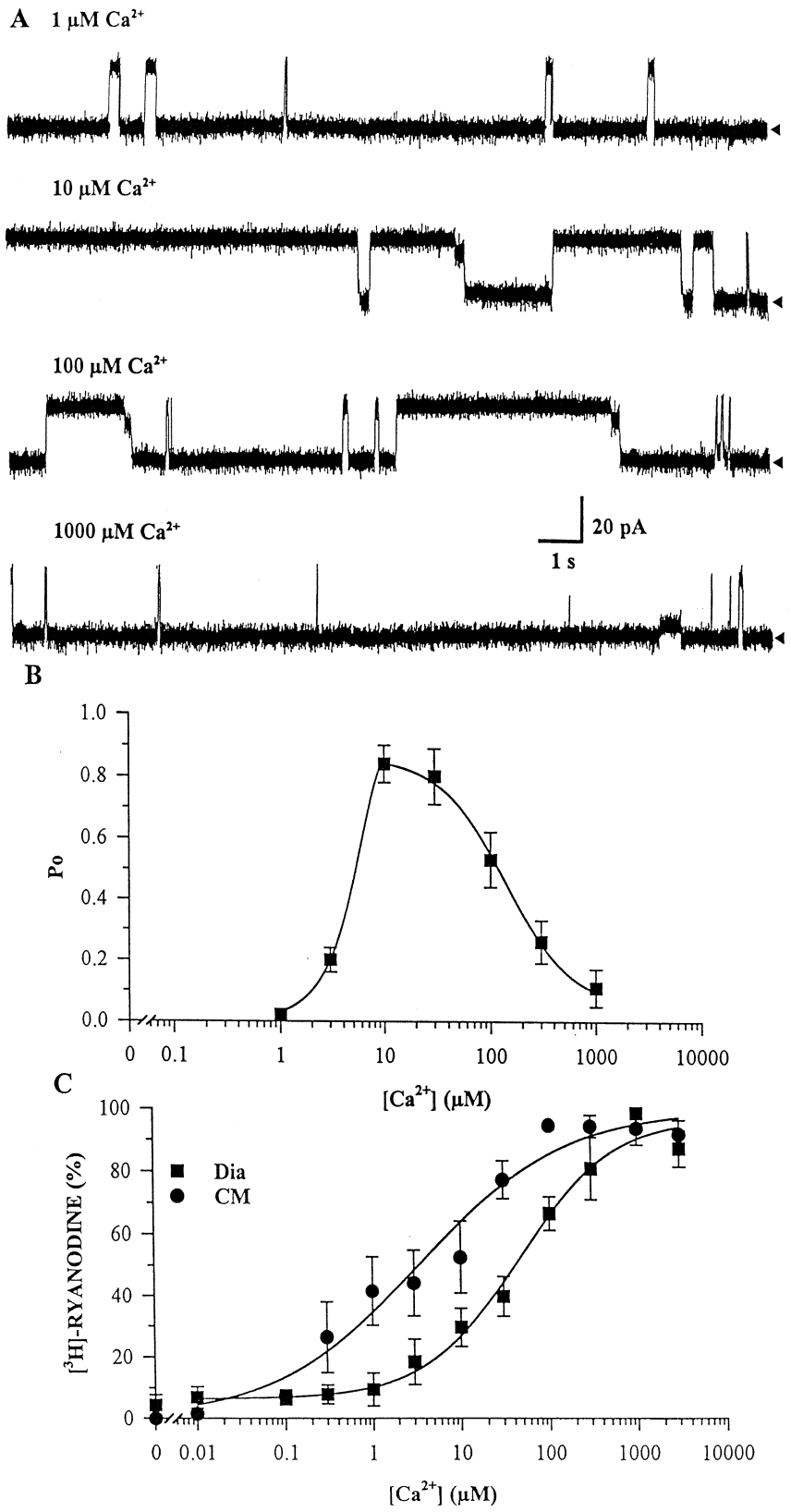
A
1 μM Ca2+
10 μM Ca2+
100 μM Ca2+
1000 μM Ca2+
20 pA
1 s
B
Po
[Ca2+] (μM)
C
[3H]-RYANODINE (%)
Dia
CM
[Ca2+] (μM)

channel in the presence of increasing concentrations of free Ca^{2+}. The open probability (P_o) of the channel was very low in 1 μM Ca^{2+} ($P_o = 0.05$), characterized by short open events. The channel was maximally activated by 10 μM Ca^{2+} ($P_o = 0.80$), and was gradually inactivated at higher concentrations, to display only spike-like openings in 1 mM Ca^{2+} ($P_o = 0.09$). Fig. 4 also indicates that the channel unitary conductance was not affected by successive changes in Ca^{2+} concentration. Fig. 4B summarizes the relationship between cytoplasmic Ca^{2+} and the P_o of the channel. Activity threshold was recorded with 1 μM Ca^{2+}. The channel was activated by micromolar Ca^{2+} and inactivated by concentrations above 30 μM Ca^{2+}. Threshold activation of skeletal and cardiac channels in 50/250 mM *trans/cis* $CsCH_3SO_3$ both fall in the range 0.1–10 μM Ca^{2+} [20,58]. In contrast, the skeletal channel was in average 20-fold more sensitive to inactivation by high [Ca^{2+}] than the cardiac channel, with threshold inhibitions of 100 μM and 1–2 mM, respectively [20,58]. Thus, the sensitivity of the diaphragm SR Ca^{2+}-release channel to high [Ca^{2+}] is similar to that of the skeletal SR channel.

Micromolar Ca^{2+} concentrations significantly increased [^{3}H]rya-nodine binding to the diaphragm and cardiac SR (Fig. 4C). Diaphragm SR was less sensitive to Ca^{2+} than cardiac SR. The threshold for detection of ryanodine binding was around 5 μM Ca^{2+} for the diaphragm, compared to less than 0.3 μM Ca^{2+} for the cardiac SR. Half-maximal binding (EC_{50}) was reached with 40.0 μM and 3.5 μM free Ca^{2+}, respectively. Similar Ca^{2+}-dependent [^{3}H]ryano-dine binding relationships have been reported in the literature for the cardiac SR Ca^{2+}-release channel, with half-maximal binding around 1 μM Ca^{2+} [52,47]. In contrast, Zimanyi and Pessah [62] demonstrated that ryanodine binding was less sensitive to Ca^{2+} in skeletal SR than in cardiac SR, with EC_{50} values of 50 and 1 μM, respectively. These results also support a similar Ca^{2+} sensitivity for the diaphragm and skeletal SR membranes.

3.4. Activation by ATP and inhibition by Mg^{2+}

The modulating effects of ATP and Mg^{2+} on the diaphragm SR Ca^{2+}-release channel are illustrated in Fig. 5A. Channel fusions were initially performed in 50/250 mM *trans/cis* $CsCH_3SO_3$ and 1 μM free Ca^{2+}. Under these conditions, the channel displayed a relatively low activity characterized by short open events ($\leq$ 10 ms). The channel was maximally activated by addition of 2 mM ATP to the *cis* chamber. Then, Mg^{2+} modified the channel activity and gating in a manner which was similar to that reported for other SR Ca^{2+}-release channels [18]. With increasing [Mg^{2+}], long open events were gradually replaced by very brief events separated by long closed events. The fact that Mg^{2+} induced a rapid flickering of Ca^{2+}- and ATP-activated channels suggests that the cation may partially obstruct the pore [15]. Fig. 5B summarizes the effect of Mg^{2+} on the channel P_o. A sigmoid relationship was obtained by plotting steady-state P_o values against the logarithm of free [Mg^{2+}] *cis*. The 50% inhibitory concentration (IC_{50}) was estimated at 100 μM Mg^{2+}, and complete channel inactivation was observed with 3 mM Mg^{2+}. Similarly, 3 to 5 mM free Mg^{2+} was shown to prevent Ca^{2+} activation and to depress P_o in Ca^{2+}/ATP-activated skeletal channels [63]. Cardiac SR Ca^{2+}-release channels were reported to be less sensitive to Mg^{2+} than skeletal SR channels, with threshold inhibition and IC_{50} values of approximately 0.3 and 1 mM, respectively [56].

We also compared the effect of Mg^{2+} on the binding of nanomolar [^{3}H]ryanodine to the di-

Fig. 4. Calcium sensitivity of the Ca^{2+}-release channel activity and ryanodine binding to the diaphragm SR. (A) Unitary current recordings measured at a holding potential of +50 mV in 50/250 mM *trans/cis* $CsCH_3SO_3$, 20 mM Tris–HEPES (pH 7.4) and increasing concentrations of free Ca^{2+} in the *cis* chamber. Arrowheads on the right indicate the zero-current level. (B) Concentration-response curve of the effects of free Ca^{2+} *cis* on the diaphragm channel open probability (P_o), performed under the experimental conditions described above. Data points represent average values ($\pm$SEM) from four or five experiments. Free Ca^{2+} concentrations were calculated by a computer program provided by Dr. Fabiato [43]. (C) Percent [^{3}H]ryanodine binding to the diaphragm (DIA) and cardiac (CM) SR membrane enriched fractions as a function of free Ca^{2+} concentration ($n = 4$). Average values ($\pm$SEM) were expressed in percent of maximum binding capacity: 1.2 pmol/mg protein for the diaphragm and 2.2 pmol/mg protein for the cardiac SR membranes. Ryanodine binding was less sensitive to Ca^{2+} in diaphragm SR than in cardiac SR.

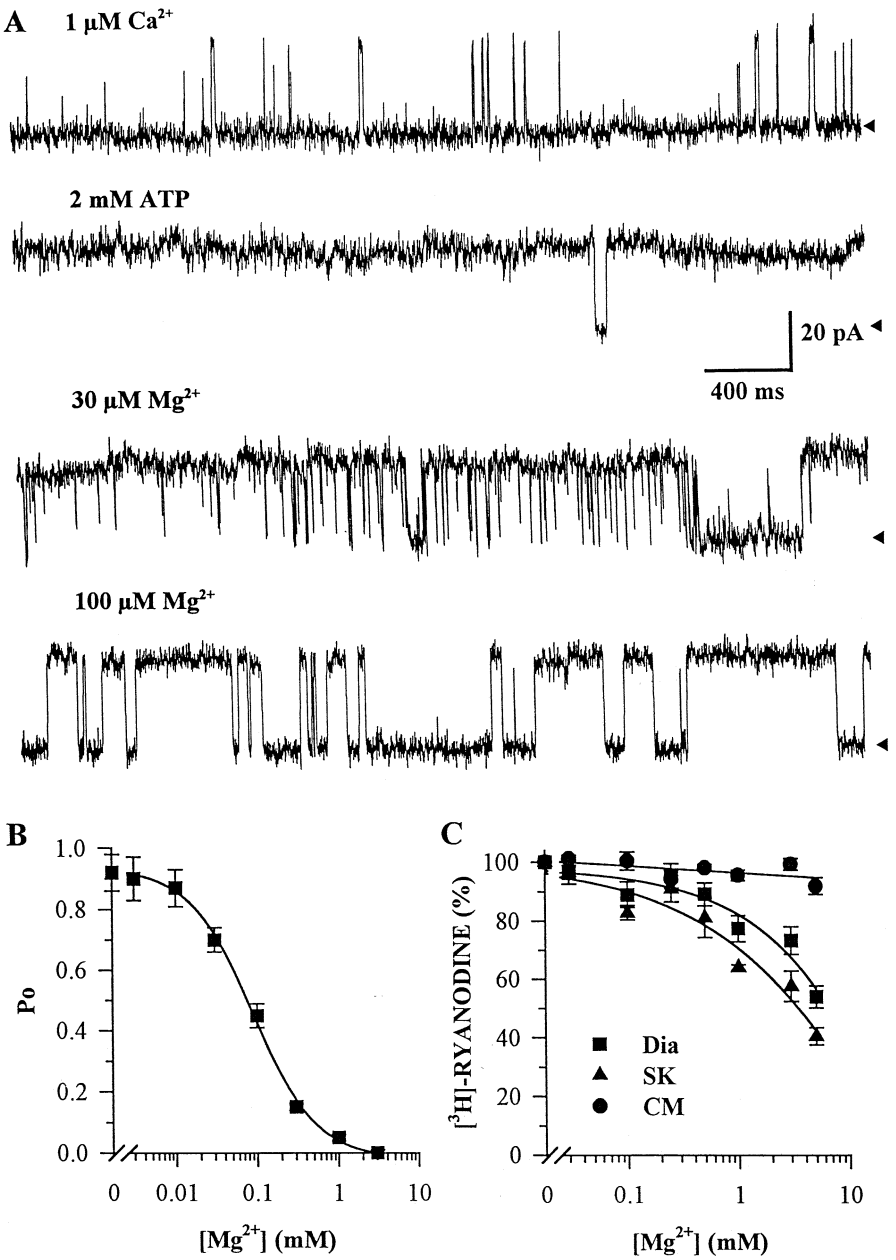

Fig. 5. Magnesium sensitivity of the Ca^{2+}-release channel activity and ryanodine binding to the diaphragm SR. (A) Unitary current recordings measured at a holding potential of +60 mV in 50/250 mM *trans/cis* $CsCH_3SO_3$,1 μM free Ca^{2+} and 20 mM Tris–HEPES (pH 7.4). Under these conditions, channel activity was minimal (first trace). The channel was activated by addition of 2 mM Na_2ATP *cis* (second trace) and then inhibited by sequential addition of 0 to 300 μM free Mg^{2+} to the *cis* chamber (lower traces). (B) Concentration-dependent effects of free Mg^{2+} *cis* on the P_o of the diaphragm channel, performed under the experimental conditions described above. Data points represent average values (±SEM) from six experiments. (C) Normalized percent [^{3}H]ryanodine binding to the native diaphragm (■), skeletal (▲) and cardiac (●) SR Ca^{2+}-release channels as a function of $MgSO_4$ concentration ($n = 4$). Average values (±SEM) were expressed in percent of the maximum binding capacity for each preparation (1.2, 2.2 and 3.5 pmol/mg protein for the diaphragm, cardiac and skeletal SR membranes, respectively). Note that [^{3}H]ryanodine binding to the diaphragm and skeletal muscle SR channels decreased with increasing concentration, but this was not the case for the cardiac SR.

aphragm, skeletal and cardiac SR (Fig. 5C). [^{3}H]ryanodine binding to the diaphragm and skeletal channels gradually decreased with increasing concentrations of Mg^{2+}, with IC_{50} values estimated at 5 and 3 mM Mg^{2+}, respectively. In contrast, [^{3}H]ryanodine binding to the cardiac channel remained above 90% with Mg^{2+} concentrations as high as 10 mM. In the literature, [^{3}H]ryanodine binding to the cardiac channel was also found to be less sensitive to Mg^{2+} than the skeletal channel [17,18,62]. Therefore, based on Mg^{2+} sensitivity, the diaphragm channel would be classified as a skeletal isoform.

3.5. Inhibition of the Ca^{2+}-release channel by micromolar ryanodine

Fig. 6 shows the behavior of a single channel recorded in 50/250 mM *trans/cis* $CsCH_3SO_3$ and 1

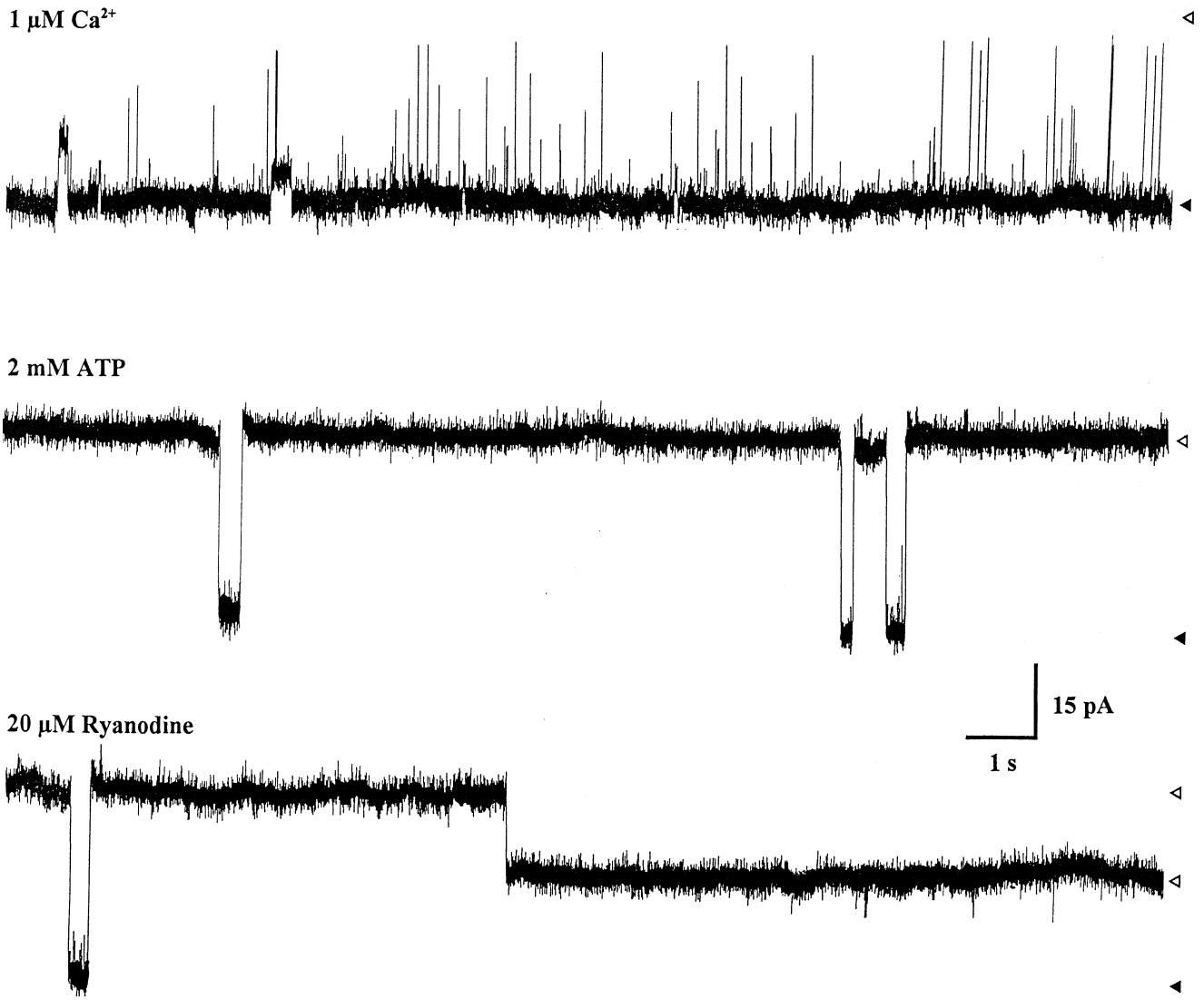

Fig. 6. Effect of ryanodine on the diaphragm SR Ca^{2+}-release channel. Unitary current recordings measured at a holding potential of +60 mV in 50/250 mM *trans/cis* $CsCH_3SO_3$, 1 μM free Ca^{2+}, 20 mM Tris–HEPES at pH 7.4 (upper trace). The channel was maximally activated by 2 mM Na_2ATP *cis* (middle trace). Within 1–2 min after addition to the *cis* chamber, ryanodine blocked the channel into a subconducting state (lower trace).

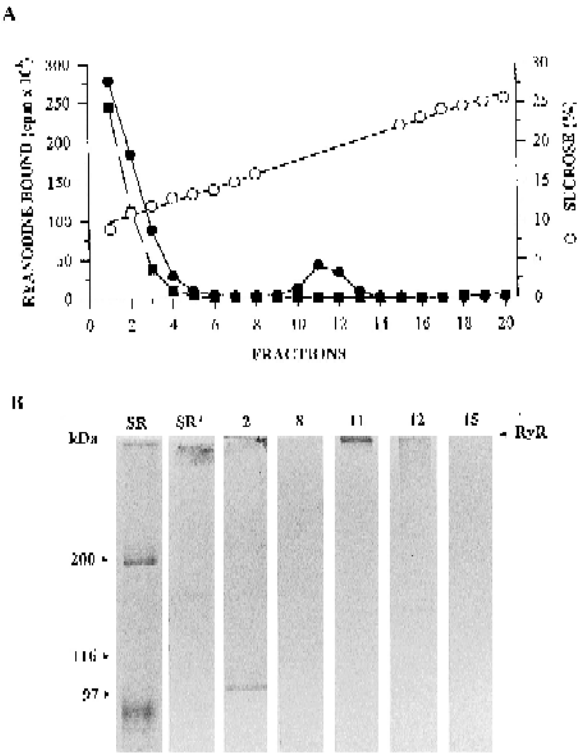

Fig. 7. Analysis of protein fractions collected from the sucrose gradient used to purify the ryanodine receptor. (A) [^{3}H]ryanodine sedimentation profile following centrifugation of solubilized SR membranes on a 5–25% sucrose gradient. The open symbols indicate the percent sucrose determined in the corresponding fractions. (●) Total and non-specific (■) [^{3}H]ryanodine binding. Notice the absence of specific [^{3}H]ryanodine binding in fractions 11 and 12 in the presence of excess cold ryanodine (5 mM). (B) SDS-PAGE analysis of SR membranes (SR), SR membranes solubilized (SR*) and fractions collected from the sucrose gradients prior to and following solubilization and purification of the ryanodine receptor. Equal amounts of proteins were subjected to SDS-PAGE on a 6% gel and stained with Coomassie blue. Molecular weight standards and the ≈ 400 kDa ryanodine receptor (RR) are indicated by arrowheads.

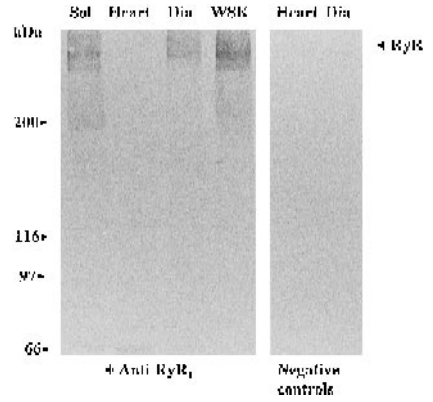

Fig. 8. Comparative immunoblot analysis of the protein profiles of cardiac, skeletal and diaphragm muscle SR membranes. Microsomal fractions isolated from canine soleus (Sol), heart (Heart), diaphragm (Dia) and rabbit white skeletal (WSK) muscles were subjected to SDS-PAGE and transferred to nitro-cellulose membranes. Immuno-staining was performed with skeletal anti-RyR$_1$ polyclonal antibodies (Section 2). On the right are shown the negative controls performed on canine cardiac and diaphragm SR fractions in the absence of primary antibody. Arrows and numbers represent the positions and the values (kDa) of the molecular weight standards, respectively. The skeletal anti-RyR$_1$ antibodies reacted with a ~400 kDa protein band in the diaphragm, soleus and WSK SR membranes.

μM free Ca^{2+}. Under these conditions, the channel activity was very low ($P_o = 0.02$), characterized by spike-like openings. The channel was activated by 2 mM ATP *cis* ($P_o = 0.87$) and then inhibited by 20 μM ryanodine *cis*. Within 1–2 min after addition of ryanodine to the *cis* chamber, the channel was blocked into a subconductance state. Similar modifications were reported for skeletal and cardiac SR Ca^{2+}-release channels [64].

Fig. 9. Biophysical properties and electrophysiological characterization of the purified diaphragm SR ryanodine receptor reconstituted into planar lipid bilayers. (A) Single channel activity recorded at various holding potentials in symmetrical 200 mM KCl, 100 μM free Ca^{2+}, 20 mM K–HEPES (pH 7.4) and 1 mM Na_2ATP *cis*. (B) Current/voltage relationships in 200/200 mM and 200/300 mM *trans/cis* KCl, with respective mean (±SEM) conductances of 703 ± 15 pS and 727 ± 21 pS ($n = 3$). The reversal potential was shifted toward the calculated equilibrium potential in asymmetrical buffer systems. (C) Average P_o values (±SEM) as a function of the applied voltage for the purified ryanodine receptor (●) and the native Ca^{2+}-release channel (■), measured in symmetrical 200 mM KCl, 20 mM K–HEPES (pH 7.4), plus 100 μM free Ca^{2+} and 2 mM Na_2ATP *cis* and in 50/250 mM *trans/cis* $CsCH_3SO_3$, 20 mM Tris–HEPES (pH 7.4), plus 10 μM free Ca^{2+} and 2 mM Na_2ATP *cis*, respectively ($n = 5$). Open probability values increased from 0.6 to 1.0 with depolarizing voltages.

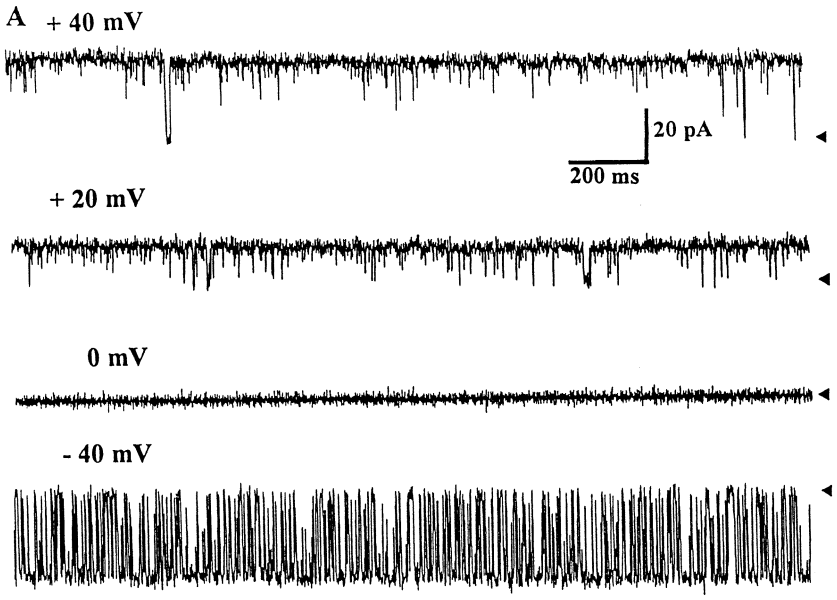
A
+ 40 mV
20 pA
200 ms
+ 20 mV
0 mV
- 40 mV

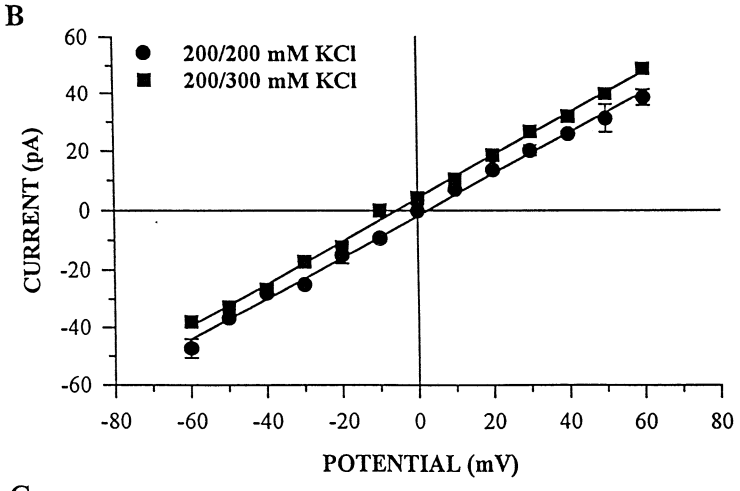
B
200/200 mM KCl
200/300 mM KCl
CURRENT (pA)
POTENTIAL (mV)

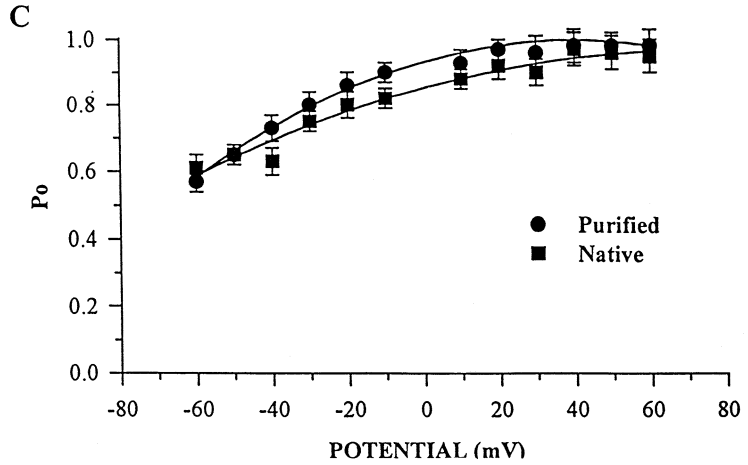
C
Po
Purified
Native
POTENTIAL (mV)

3.6. Purification of the diaphragm SR Ca^{2+}-release channel

The Ca^{2+}-release channel was solubilized from SR membrane vesicles with 1% CHAPS and 3% Azolectine (1 M NaCl, 5 mM AMP, 50 μM free Ca^{2+} and 170 nM [^{3}H]ryanodine), and purified by ultracentrifugation in a linear 5–25% (w/v) sucrose density gradient. The resulting fractions, as well as solubilized SR membranes, were analyzed for [^{3}H]ryanodine binding activity and protein content. A single peak of radioactivity was detected in 17–19% sucrose (Fig. 7A), as previously determined for the cardiac and skeletal SR membranes [7,12]. Radioactivity in fractions 15–20 was decreased close to the background level when the solubilized membranes were incubated with 5 μM cold ryanodine. The large amount of radioactivity at the top of the gradient corresponded to unbound [^{3}H]ryanodine. SDS-PAGE analysis indicated specific comigration of a single high molecular weight polypeptide of $\sim$400 kDa in the SR microsomal fractions before and after solubilization. This protein band was only detected in the [^{3}H]ryanodine binding fractions, 11 and 12 (Fig. 7B). The 400 kDa protein has been previously identified as the monomeric component of the Ca^{2+}-release

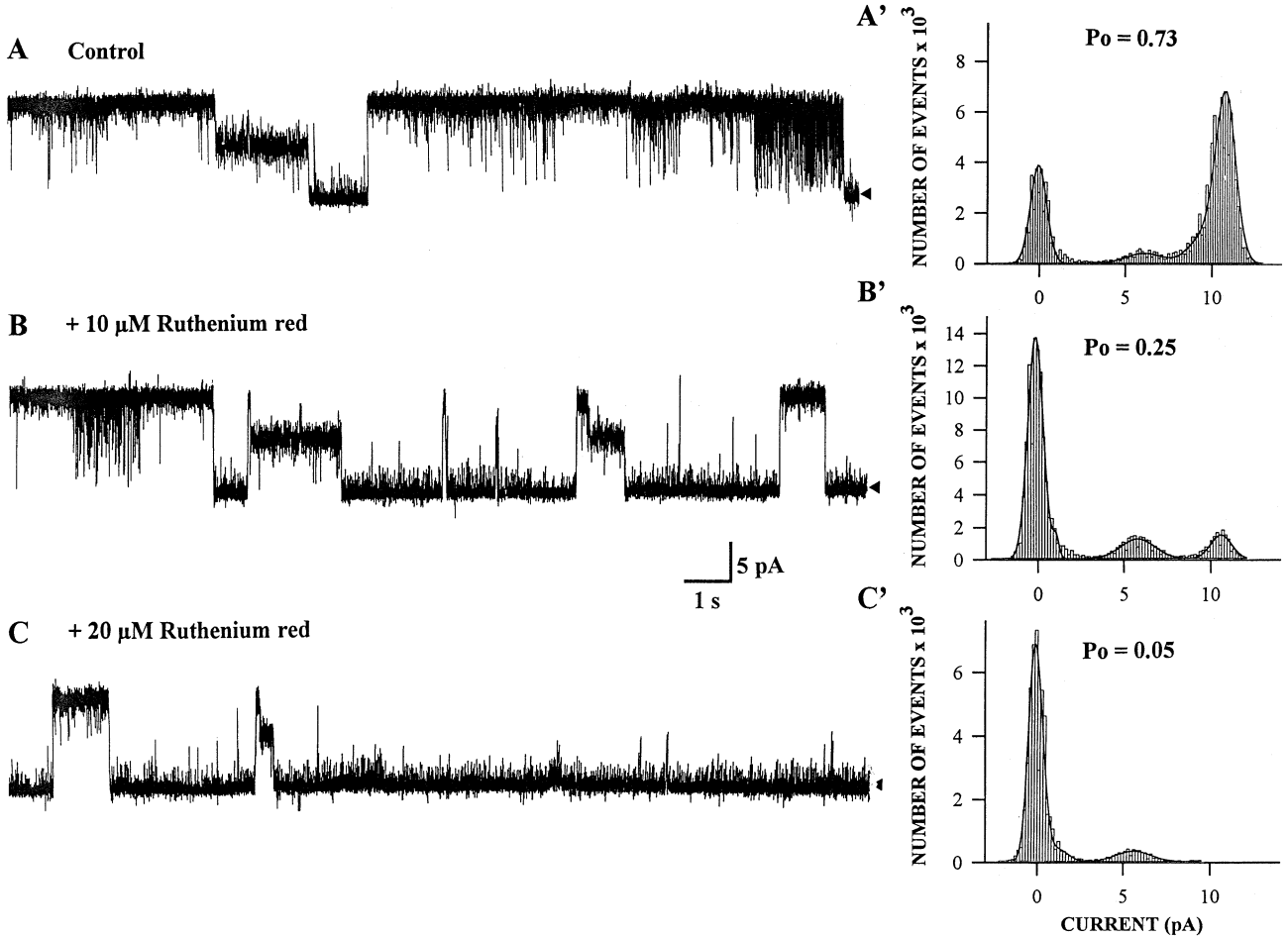

Fig. 10. Ruthenium red inhibition of the purified and reconstituted diaphragm SR Ca^{2+} channel. Single channel activity recorded in symmetrical 200 mM KCl, 20 mM K-HEPES (pH 7.4), 100 μM free Ca^{2+} and 1 mM Na_2ATP *cis*, at a holding potential of +40 mV. (A) Control channel activity in the absence of ruthenium red. (B) Partial inhibition of the current with 10 μM ruthenium red *cis*. (C) The channel activity was further inhibited by 20 μM ruthenium red *cis*. Complete inhibition occurred 25 s after the addition of ruthenium red 20 μM *cis*. (A′), (B′) and (C′) are corresponding amplitude histograms from 1 min data files. P_o values represent the fraction of time spent by the channel in the fully-open and subconducting states.

channel [12]. Minor contaminations, probably by the 205 kDa myosin and the 160–176 kDa α_1- and α_2-subunits of the dihydropyridine receptor, were occasionally detected in fractions 11 and 12, in which cases the protein fraction was further purified on a heparine-sepharose affinity column [47]. Most of the other SR proteins, such as the 100 kDa Ca^{2+}, Mg^{2+}-ATPase [65] and/or triadin [66], remained at the top portion of the sucrose density gradient.

The identity of the purified protein was further assessed with a polyclonal antibody raised against the skeletal RyR_1 isoform (provided by Dr. Meissner). Membrane fractions were prepared from canine slow-twitch soleus muscles, heart, diaphragm, and rabbit fast-twitch white skeletal (WSK) muscles, as described in Section 2. The antibody recognized a $\sim$400 kDa protein band in the diaphragm, the slow-twitch soleus and in fast-twitch WSK muscles, but not in cardiac muscles (Fig. 8). Additional protein bands which migrated at $\sim$300 and $\sim$200 kDa were occasionally detected. Most likely their appearance was due to partial degradation of the $\sim$400 kDa band by endogenous proteases [12,67].

3.7. Biophysical properties of the purified Ca^{2+}-release channel

The purified diaphragm ryanodine receptor (RyR), added to the *cis* chamber, incorporated itself into the PLB in such a way that the regulatory sites located on the cytoplasmic side of the channel are exposed to the *cis* chamber. In all reconstitution experiments, the purified complex was incorporated in symmetrical 200 mM KCl, 20 mM K–HEPES, 10 or 100 μM free Ca^{2+} and 1–2 mM ATP *cis*. The choice of buffer was motivated by the finding that symmetrical monovalent buffer systems facilitate reconstitution of skeletal and cardiac purified RyR, and that larger unitary currents were recorded with K^+ or Na^+ than with Ca^{2+} as the permeant cation [7,12,54,60]. Fig. 9A shows typical unitary current recordings of a RyR, characterized by the predominance of long open states with frequent incomplete transitions into the closed state [10]. The channels displayed an extremely high conductance (714 ± 22 pS), as reported for cardiac [68,69] and skeletal isoforms [68,70] in 250 mM KCl. The shift in reversal potential toward negative voltages in 200/300 mM *trans*/*cis* KCl argues in favor of a cation selectivity with respect to Cl^- anions (Fig. 9B). Thus, the purified canine diaphragm RyR functions as a cation-selective channel following reconstitution into PLB, as previously shown for the purified skeletal RyR [12,54].

Voltage sensitivity of the native and purified diaphragm SR Ca^{2+}-release channels were compared over the same range of potentials in the presence of symmetrical 10 μM free Ca^{2+} and 1 mM ATP *cis*. The native and purified channels displayed similar low voltage dependency, P_o values increasing from 0.5 to 0.9 with depolarizing voltages (Fig. 9C). Rousseau and Meissner [19] reported P_o values increasing from 0.25 to 0.65 at voltages from -40 to $+20$ mV, with 2.5 mM cytoplasmic free Ca^{2+} and 50 mM Ca^{2+} *trans* as the permeant ion. The lower P_o values would be explained by the absence of ATP in their buffers [18,19,41,71].

3.8. Inhibition of the purified Ca^{2+}-release channel by ruthenium red

We examined the gating behavior and P_o of the purified diaphragm RyR reconstituted in PLB following the addition of micromolar ruthenium red. Single-channel fluctuations were initially recorded in 200 mM KCl, 100 μM free Ca^{2+} and 1 mM ATP *cis* (Fig. 10A). Addition of 10 μM ruthenium red to the *cis* chamber did not affect the channel conductance, but long closed events and subconductance states of about half-maximal conductance were frequently observed (Fig. 10B). The channel P_o decreased from 0.73 (Fig. 10A′) to 0.25 (Fig. 10B′). Complete and irreversible inhibition of the channel activity was obtained with 20 μM ruthenium red within 25 s (Fig. 10C and C′). In the literature, 1 to 30 μM ruthenium red were also shown to completely abolish the activity of both native and purified cardiac and skeletal channels in PLB [7,12,41,56].

4. Discussion

Electrical coupling between surface membrane depolarization and SR Ca^{2+} release in skeletal and cardiac muscles involves two different mechanisms. In cardiac muscle, extracellular Ca^{2+} enters through

voltage-sensitive DHPRs located in the T-tubules and activates SR RyRs, a mechanism referred to as Ca^{2+}-induced Ca^{2+} release [25]. In skeletal muscle, the DHPRs would be 'physically' linked to the RyRs, an activation independent of extracellular Ca^{2+} entry [23,24]. Although classified as a skeletal muscle, the diaphragm appears to be functionally closer to the myocardium. They both contract rhythmically for life, and extracellular Ca^{2+} plays an important role in force generation [72]. These particularities could involve differences in the ECC machinery of the diaphragm, compared to other skeletal muscles.

In this study, we describe the biochemical and biophysical properties of the native and purified diaphragm SR Ca^{2+}-release channel. Ryanodine, the specific marker of SR Ca^{2+}-release channels [3,4], was shown to bind to diaphragm SR membranes with K_D and B_{max} values similar to those of cardiac and skeletal SR [13,21,47–50]. Incorporation of SR vesicles into PLB yielded large conductance Cs^+ currents, which were affected by the same factors that modulate the Ca^{2+}-release channels of cardiac and skeletal SR, namely ryanodine, Ca^{2+}, Mg^{2+} and ATP [15]. The channel was purified as a 400 kDa protein on SDS-PAGE, a band previously identified as the monomeric component of the RyR in rabbit skeletal muscle [12]. Reconstitution of the purified channel into PLB yielded current conductances above 700 pS in KCl, as reported for the other isoforms [54,55]. The purified channel exhibited gating properties typical to RyRs, retained the P_o/voltage dependence of the native channel and was inhibited by micromolar ruthenium red [15].

We provide evidence that the properties of the diaphragm SR Ca^{2+}-release channel correspond closely to those of skeletal muscle RyRs. First, the IC_{50} of [^{3}H]ryanodine binding to diaphragm SR by ryanodine was within the range reported for skeletal SR (18–22 nM) [10], but higher than the IC_{50} (5.2 nM) reported for cardiac SR [39]. Second, EC_{50} for ryanodine binding to diaphragm SR was reached with 40 μM Ca^{2+}, which is in the range as reported for skeletal SR [62], but higher than values estimated for cardiac SR in this study (3.5 μM) and elsewhere (1 μM) [47,52]. Third, ryanodine binding sensitivity to millimolar Mg^{2+} was higher for the diaphragm and skeletal SR than for cardiac SR [17,18,62]. The channel sensitivity to Ca^{2+} and Mg^{2+} in PLB corroborated these findings. Threshold inhibition by cytoplasmic Ca^{2+} was 30–100 μM, which is in the same range of skeletal isoform, but 20-fold lower than reported for the cardiac channel [20,58]. And Ca^{2+} release was completely abolished by 3–5 mM Mg^{2+}, as reported for skeletal channels [63]. Therefore, based on ryanodine-binding and gating properties, the diaphragm would be classified as a skeletal muscle.

The data presented in this study could not account for the high sensitivity of diaphragm muscle contraction to extracellular Ca^{2+}. However, recent findings on the distribution of the different RyR isoforms in vertebrates suggest that ECC may be far more sophisticated than anticipated from current recordings of cardiac and skeletal channels in PLB, or $^{45}Ca^{2+}$-loaded SR vesicles. Until recently, it was generally believed that mammalian tissues express a cardiac isoform (RyR_2), a skeletal isoform (RyR_1) and a brain isoform also present in smooth muscles (RyR_3). More sensitive mRNA techniques and isoform-specific antibodies have allowed the detection of more than one isoform in most tissues, including muscles, glands and the brain [73,74]. Cardiac muscles express RyR_2 and RyR_3, whereas skeletal muscles express RyR_1 and RyR_3 [74]. In skeletal muscles, while RyR_1 was expressed at high levels, RyR_3 content was found highly variable [75]. This isoform was more abundant in the diaphragm and soleus than in the tibialis anterior and abdominal muscles and no RyR_3 was detected in fast-twitch extensor digitorum longus (EDL). Interestingly, the relative content of skeletal muscles in RyR_3 reflects their sensitivity to extracellular Ca^{2+}. Twitch tension of diaphragm and cardiac muscle fibers was abolished 3 and 10 min after removal of extracellular Ca^{2+}, respectively. In contrast, twitch tension of soleus and EDL muscles were at 62 and 75% of control fibers after a 30 min zero-Ca^{2+} exposure [72]. These findings suggest that RyR_3 could be involved in SR Ca^{2+}-induced Ca^{2+} release. In support of this, ultrastructural and ligand binding studies indicate that in skeletal muscles, not all RyRs are mechanically coupled to DHPRs [2,15]. Mice that carry a null mutation for the RyR_1 gene lack electrical coupling in their skeletal myocytes [76]. These cells still responded to caffeine by SR Ca^{2+} release equivalent to one-tenth of the level measured in normal mice, which probably corresponded to the activity of RyR_3 [76]. Therefore,

RyR_1 would be coupled to DHPRs, while RyR_3 would be Ca^{2+}-gated Ca^{2+} channels. A similar hypothesis was drawn by comparing cDNA sequences of mammalian and nonmammalian RyRs. The 'skeletal-like' α-isoform and the 'cardiac-like' β-isoform of frog and chicken skeletal muscles were found most homologous to RyR_1 and RyR_3 isoforms, respectively [77,78].

The two RyR isoforms expressed in skeletal muscles have not been distinguished so far on the basis of electrophysiological properties [1,2,15]. A possible explanation would be that the ratio of RyR_3/RyR_1 is too low for RyR_3 to be detected and identified in PLB. However, it is unlikely to be the case for the diaphragm, where RyR_3 was found particularly abundant. An alternative explanation would be that the two isoforms coexist in RyR heterotetramers, and that the biophysical properties of the SR Ca^{2+}-release channel recorded in PLB represent the overall contribution of the two isoforms. The mechanism by which voltage-gated and Ca^{2+}-gated RyRs may interact has been investigated by Klein et al. [79] using voltage-clamp and confocal imaging techniques on frog skeletal muscles. They proposed that a local rise in Ca^{2+} concentration generated by the voltage-gated α-RyRs would activate nearby ligand-gated β-RyRs, giving rise to a stochastic pattern of Ca^{2+}-release events. Yet the existence of a similar mechanism in mammalian tissues is being questioned, since RyR_3 is often expressed in much lower level than RyR_1. Whether they exist as homotetramers or heterotetramers, they would have to be restricted to specific regions of SR membranes in order to play a significant role in ECC. Further studies are warranted to elucidate the functional implications of mixed populations of RyRs in ECC of mammalian skeletal muscles as vital as the diaphragm.

Acknowledgements

This study was supported by grants from HSFC and CRM of Canada. Dr. E. Rousseau is a senior FRSQ scholar and Dr. M. Picher is a recipient of an FRSQ research fellowship. The authors would like to thank Dr. P. Pape for his valuable suggestions in preparing the manuscript.

References

[1] E. Rios, G. Pizzaro, Physiol. Rev. 71 (1991) 849–908.
[2] W. Melzer, A. Herrmann-Frank, H.C. Luttgau, Biochim. Biophys. Acta 1241 (1995) 59–116.
[3] S. Fleischer, E.M. Ogunbunmi, M.C. Dixon, E.A.M. Fleer, Proc. Nat. Acad. Sci. USA 82 (1985) 7256–7259.
[4] I.N. Pessah, A.O. Francini, D.J. Scales, A.L. Waterhouse, J.E. Casida, J. Biol. Chem. 262 (1986) 8643–8648.
[5] H. Takeshima, S. Nishimura, T. Matsumoto, H. Ishida, K. Kangawa, N. Minamino, H. Matsuo, M. Ueda, Hanaoka, T. Hirose, S. Numa, Nature London 339 (1989) 439–445.
[6] M. Inui, A. Saito, S. Fleischer, J. Biol. Chem. 262 (1987) 1740–1747.
[7] K. Anderson, F.A. Lai, Q.-Y. Liu, E. Rousseau, H.P. Erickson, G. Meissner, J. Biol. Chem. 264 (1989) 1329–1335.
[8] Y. Hakamata, J. Nakai, H. Takeshima, K. Imoto, FEBS Lett. 312 (1992) 229–235.
[9] G. Meissner, E. Rousseau, F.A. Lai, Q.-Y. Liu, K.A. Anderson, Mol. Cell. Biochem. 82 (1988) 59–65.
[10] T. Imagawa, J.S. Smith, R. Coronado, K.P. Campbell, J. Biol. Chem. 262 (1987) 16636–16643.
[11] M. Inui, A. Saito, S. Fleischer, J. Biol. Chem. 262 (1987) 15637–15642.
[12] F.A. Lai, H.P. Erickson, E. Rousseau, Q.-Y. Liu, G. Meissner, Nature 331 (1988) 315–319.
[13] F.A. Lai, M. Misra, L. Xu, H.A. Smith, G. Meissner, J. Biol. Chem. 264 (1989) 16776–16785.
[14] F.A. Lai, K.A. Anderson, E. Rousseau, Q.-Y. Liu, G. Meissner, Biochem. Biophys. Res. Commun. 151 (1988) 441–449.
[15] G. Meissner, Ann. Rev. Physiol. 56 (1994) 485–508.
[16] J. Nakai, T. Imagawa, Y. Hakamat, M. Shigekawa, H. Takeshima, S. Numa, FEBS Lett. 271 (1990) 169–177.
[17] I.N. Pessah, A.L. Waterhouse, J.E. Casida, Biochim. Biophys. Res. Commun. 128 (1985) 449–456.
[18] J.S. Smith, R. Coronado, G. Meissner, J. Gen. Physiol. 88 (1986) 573–588.
[19] E. Rousseau, G. Meissner, Am. J. Physiol. 256 (1989) H328–H333.
[20] A. Chu, M. Fill, E. Stefani, M.L. Entmann, J. Membr. Biol. 135 (1993) 49–59.
[21] M.A. Strand, C.F. Louis, J.R. Mickelson, Biochim. Biophys. Acta 1175 (1993) 319–326.
[22] J. Hain, H. Onoue, M. Mayrleitner, S. Fleischer, H. Schindle, J. Biol. Chem. 270 (1995) 2074–2081.
[23] W.A. Catterall, Cell 64 (1991) 871–874.
[24] A. Fabiato, J. Gen. Physiol. 78 (1981) 457–497.
[25] M.D. Stern, Biophys. J. 63 (1992) 497–517.
[26] D.F. Rochester, J. Clin. Invest. 75 (1985) 1397–1402.
[27] J.A. Burbach, E.H. Schlenker, J.L. Johnson, Am. J. Physiol. 253 (Reg. Int. Comp. Physiol. 22) (1987) R275–284.
[28] D. Chemla, E. Scalbert, P. Desche, J.-C. Pourny, F. Lambert, Y. Lecarpentier, J. Pharmacol. Exp. Ther. 262 (1992) 516–525.

[29] K.-S. Hsu, J.-J. Kang, S.-Y. Lin-Shiau, Jpn. J. Pharmacol. 62 (1993) 161–168.
[30] C. Coirault, D. Chemla, N. Pery-Man, I. Suard, S. Salmeron, Y. Lecarpentier, J. Appl. Physiol. 76 (1994) 1468–1475.
[31] I. Kimura, M. Kimura, M. Kimura, Jpn. J. Pharmacol. 44 (1987) 510–513.
[32] Y. Lecarpentier, N. Pery, C. Coirault, E. Scalbert, P. Desche, I. Suard, F. Lambert, D. Chemla, Am. Heart J. 126 (1993) 770–776.
[33] P. Herve, Y. Lecarpentier, F. Brenot, M. Clergue, D. Chemla, P. Duroux, J. Appl. Physiol. 65 (1988) 1950–1956.
[34] J.H. Zavecz, W.M. Anderson, J. Appl. Physiol. 73 (1992) 30–35.
[35] M. Anger, F. Lambert, D. Chemla, P. Desche, E. Scalbert, A.-M. Lompre, Y. Lecarpentier, Am. J. Physiol. 268 (Heart Circ. Physiol 5/2) (1995) H1947–H1953.
[36] M. Picher, A. Decrouy, E. Rousseau, Biochim. Biophys. Acta 1279 (1996) 93–103.
[37] E. Rousseau, J. Pinkos, D. Savaria, Can. J. Physiol. Pharmacol. 70 (1992) 394–402.
[38] O.H. Lowry, N.J. Rosebrough, A.L. Fan, R.J. Rendall, J. Biol. Chem. 193 (1951) 65–275.
[39] M.J. Hawkes, M. Diaz-Munoz, S.L. Hamilton, Membr. Biochem. 8 (1989) 133–145.
[40] A. Decrouy, M. Juteau, S. Proteau, J. Teijeira, E. Rousseau, J. Mol. Cell. Cardiol. 28 (1996) 767–780.
[41] J.S. Smith, R. Coronado, G. Meissner, Nature 316 (1985) 46–449.
[42] E. Rousseau, J. Membr. Biol. 110 (1989) 39–47.
[43] A. Fabiato, in: S. Fleischer, B. Fleischer (Eds.), Methods in Membrane Enzymology, Academic Press, Orlando, FL 157, 1988, pp. 378–417.
[44] D.M. Bers, K.T. MacLeod, in: P.F. Baker (Ed.), Handbook of Experimental Pharmacology, Springer-Verlag, Berlin, Heidelberg, 1988, pp. 491–507.
[45] R. Sitsapesan, R.A.P. Montgomery, K.T. MacLeod, A.J. Williams, J. Physiol. 434 (1991) 469–488.
[46] D.P. Rardon, D.C. Cefali, R.D. Mitchell, S.M. Seiler, L.R. Jones, Circ. Res. 64 (1990) 779–789.
[47] T. Imagawa, T. Takasago, M. Shigekawa, J. Biochem. 106 (1989) 342–348.
[48] S.R.M. Holmberg, A.J. Williams, Biochim. Biophys. Acta 1022 (1990) 187–193.
[49] I.N. Pessah, I. Zimanyi, Mol. Pharmacol. 38 (1991) 679–689.
[50] T. Michalak, Y. Ogawa, J. Biochem. 112 (1992) 514–522.
[51] A.R.G. Lindsay, S.D. Manning, A.J. Williams, J. Physiol. 439 (1991) 463–480.
[52] L. Xu, A.H. Cohn, A.H. Meissner, Cardiovasc. Res. 27 (1993) 1815–1819.
[53] Q. Tu, P. Velez, M. Cortez-Gutierrez, M. Fill, J. Gen. Physiol. 103 (1994) 853–867.
[54] J.S. Smith, T. Imagawa, J. Ma, M. Fill, K.P. Campbell, R. Coronado, J. Gen. Physiol. 92 (1988) 1–26.
[55] J. Ma, M.B. Bhat, J. Zhao, Biophys. J. 69 (1995) 2398–2404.
[56] E. Rousseau, J.S. Smith, J.S. Henderson, G. Meissner, Biophys. J. 50 (1986) 1009–1014.
[57] H. Meves, W. Vogel, J. Physiol. 235 (1973) 224–265.
[58] D.R. Laver, L.D. Roden, G.P. Ahern, K.R. Eager, P.R. Junankar, A.F. Dulhunty, J. Membr. Biol. 147 (1995) 7–22.
[59] R.H. Ashley, A.J. Williams, J. Gen. Physiol. 95 (1990) 981–1005.
[60] Q.-Y. Liu, F.A. Lai, E. Rousseau, R.V. Jones, G. Meissner, Biophys. J. 55 (1989) 415–424.
[61] E. Buck, I. Zimanyi, J.J. Abramson, I.N. Pessah, J. Biol. Chem. 267 (1992) 23560–23567.
[62] I. Zimanyi, I.N. Pessah, J. Pharmacol. Exp. Ther. 256 (1991) 938–946.
[63] S. Fleischer, M. Inui, Ann. Rev. Biophys. Biophys. Chem. 18 (1989) 333–364.
[64] E. Rousseau, J.S. Smith, G. Meissner, Am. J. Physiol. 253 (Cell Physiol. 22) (1987) C364–C368.
[65] C.J. Brandl, N.M. Green, B. Korczak, D.H. MacLennan, Cell 44 (1986) 597–607.
[66] A.M. Corbett, A.H. Caswell, N.R. Brandt, J.P. Brunschwig, J. Membr. Biol. 86 (1985) 267–276.
[67] G. Meissner, E. Rousseau, F.A. Lai, J. Biol. Chem. 264 (1989) 1715–1722.
[68] E. Rousseau, J. Ladine, Q.-Y. Liu, G. Meissner, Arch. Biochem. Biophys. 267 (1988) 75–86.
[69] A.R.G. Lindsay, A.J. Williams, Biochim. Biophys. Acta 1064 (1991) 89–102.
[70] L. Xu, R. Jones, G. Meissner, J. Gen. Physiol. 101 (1993) 207–233.
[71] D. Meissner, A. Darling, J. Eveleth, Biochemistry 25 (1986) 236–244.
[72] N. Virès, D. Murciano, J.P. Seta, B. Dureuil, R. Pariente, M. Aubier, J. Appl. Physiol. 64 (1988) 26–30.
[73] R. Coronado, J. Morrissette, M. Sukhareva, D.M. Vaughan, Am. J. Physiol. 266 (1994) C1485–C1504.
[74] G. Giannini, A. Conti, S. Mammarella, M. Scrobogna, V. Sorrentino, J. Cell Biol. 128 (1995) 893–904.
[75] A. Conti, L. Gorza, V. Sorrentino, Biochem. J. 316 (1996) 19–23.
[76] H. Takeshima, M. Iino, H. Takekura, M. Nishi, J. Kuno, O. Minowa, H. Takano, T. Noda, Nature London 369 (1994) 556–559.
[77] H. Oyamada, T. Murayama, T. Takagi, M. Iino, N. Iwabe, T. Miyata, Y. Ogawa, M. Endo, J. Biol. Chem. 269 (1994) 17206–17214.
[78] L. Ottini, G. Marziali, A. Conti, A. Charlesworth, V. Sorrentino, Biochem. J. 315 (1996) 207–216.
[79] M.G. Klein, H. Cheng, L.F. Santana, Y.-H. Jiang, W.J. Lederer, M.F. Schneider, Nature 379 (1996) 455–458.